Engineering 56 (2026) 332–340

Contents lists available at ScienceDirect

Engineering

journal homepage: www.elsevier.com/locate/eng

Research
Agricultural Sensors—Article

An Implantable and Self-Powered Sensing System for the *In Vivo* Monitoring of Dynamic H_2O_2 Level in Plants

Chao Zhang [a], Xinyue Wu [a], Shiyun Yao [a], Yuzhou Shao [a], Chi Zhang [a], Shenghan Zhou [a], Jianfeng Ping [a,b], Yibin Ying [a,b,*]

[a] Laboratory of Agricultural Information Intelligent Sensing, College of Biosystems Engineering and Food Science, Zhejiang University, Hangzhou 310058, China
[b] Innovation Platform of Micro/Nano Technology for Biosensing, ZJU-Hangzhou Global Scientific and Technological Innovation Center, Zhejiang University, Hangzhou 311215, China

ARTICLE INFO

Article history:
Received 15 August 2023
Revised 27 October 2023
Accepted 19 November 2023
Available online 21 February 2024

Keywords:
Hydrogen peroxide
Implantable sensor
Self-powered sensing
Abiotic stress
Plants

ABSTRACT

The real-time monitoring of hydrogen peroxide (H_2O_2) is significant for understanding the working mechanism of signal molecules, breeding for stress tolerance, and diagnosing plant health. However, it remains a challenge to realize real-time monitoring of the dynamic H_2O_2 level in plants. Here, we report an implantable and self-powered sensing system for the continuous monitoring of H_2O_2 level in plants. A photovoltaic (PV) module is integrated into a sensing system to collect sunlight or artificial light in the planting environment in order to continuously power an implantable microsensor. The transmission process of the H_2O_2 signal was monitored and analyzed *in vivo*, and the time and concentration specificity of the H_2O_2 signal for abiotic stress were resolved. This implantable system provides a promising analysis tool for key signal molecules in plants and might be extended to the real-time monitoring of signaling molecules in other crops.

© 2024 THE AUTHORS. Published by Elsevier LTD on behalf of Chinese Academy of Engineering and Higher Education Press Limited Company. This is an open access article under the CC BY-NC-ND license (http://creativecommons.org/licenses/by-nc-nd/4.0/).

1. Introduction

"Wearable" plant sensors for monitoring plant health have been widely studied [1]. They can be classified into plant physiology and microclimate sensors [2–7], plant growth sensors [8–10], and chemical sensors [11–13]. Most of these sensors monitor physiological signals occurring in the later stages of stress response, so this monitoring is not timely and does not fully exploit the potential of wearable plant sensors. Timely plant health monitoring requires wearable sensors that can analysis biomarkers and indicators generated in earlier stages. Reactive oxygen species (ROS) and hormones are key signaling molecules generated in the early stages of plant stress response [14]. ROS can pass through plant cells during system signal transduction, switching different cells and tissues from a normal growth state into a stress state [1,15–17]. For example, when plants suffer from drought stress, ROS act as a second messenger to promote a change in the abscisic acid content in the plants, further leading to stomatal closure in the leaves [18]. Hydrogen peroxide (H_2O_2) is a primary ROS that mediates rapid systemic signals in plants, due to its long half-life and its capability for long-distance and transmembrane transmission [19,20]. However, the various molecular mechanisms related to H_2O_2 have not been fully revealed. Accurate and real-time monitoring of H_2O_2 in plants is crucial in studying plant stress response mechanisms and plant health status [21].

At present, there are two main H_2O_2 detection methods in plants: ① tissue slice staining [22,23] and ② spectrophotometry [17,24]. It is easy to miss the best detection window using these methods, and the results are reliant on human operation; therefore, these methods cannot meet the requirements of high-time resolution and continuous monitoring. In addition, the wounds formed by sampling are easily infected by bacteria, causing plant diseases. In recent years, the development of implantable sensors has provided promising access to the sensing of real-time health information in plants. In particular, Wu et al. [19] and Lew et al. [20] have developed a series of optical nanosensors that can be injected into plants to monitor real-time molecular information, providing dynamic, spatial, and temporal biochemical measurements in plants. Although these studies were conducted in the laboratory, they provide novel analytical tools for studying plant physiology [21]. H_2O_2 is a typical electroactive molecule, and the application of invasive electrochemical sensors in animal biomarker monitoring suggests a new approach for monitoring H_2O_2 in

* Corresponding author.
E-mail address: ybying@zju.edu.cn (Y. Ying).

https://doi.org/10.1016/j.eng.2023.11.021
2095-8099/© 2024 THE AUTHORS. Published by Elsevier LTD on behalf of Chinese Academy of Engineering and Higher Education Press Limited Company.
This is an open access article under the CC BY-NC-ND license (http://creativecommons.org/licenses/by-nc-nd/4.0/).

plants [25–27]. Therefore, implantable electrochemical sensors are expected to be developed for the *in vivo* analysis of H_2O_2 in plants. However, for electrochemical sensors implanted into plants, the power lines are not conducive to the stable fixation of the sensor, and the batteries require continuous charging or frequent battery replacement. These power supply issues limit the application of implantable wearable plant sensors [28]. Therefore, it is necessary to find an alternative power supply method for electrochemical sensors implanted into plants.

Here, we develop an implantable and self-powered sensing system for the continuous *in vivo* monitoring of dynamic H_2O_2 in tomato plants. The integrated system consists of a microsensor, a data-acquisition and -transmission module, and a photovoltaic (PV) module. The system can sustainably transmit the sensor's signal over a long distance to a multi-channel monitoring interface for visual analysis (Fig. 1(a)). The microsensor, which is based on three-dimensional (3D) porous laser-induced graphene (LIG), is the core of the sensing system; it can be inserted into a plant stem (a tomato plant in our case) to obtain real-time H_2O_2 information (Fig. 1(b)). To solve the problem of a continuous power supply, a PV module was designed and integrated with the data-acquisition and -transmission module and collects sunlight or artificial light in the planting environment to continuously power the microsensor (Fig. 1(c)). Using this self-powered system, the transmission process of the H_2O_2 signal was monitored *in vivo*, and the time and concentration specificity of the H_2O_2 signal for abiotic stress were investigated.

2. Materials and methods

2.1. Materials and instruments

Polyimide (PI) film (80 μm thick) and PI tapes (50 μm thick) were purchased from DuPont™ (USA). Ag/AgCl ink (E2414) was purchased from Ercon, Inc. (USA). K_2PtCl_4 and potassium iodide (KI) were purchased from Sigma Aldrich (USA). Anhydrous sodium sulfate (Na_2SO_4) and polyethylene glycol (PEG)-6000 were purchased from Macklin Inc. (China). Trichloroacetic acid (TCA) was obtained from Fuchen Chemical Reagent Co., Ltd. (China). H_2O_2 (30%) was purchased from Sinopharm Chemical Reagent Co., Ltd. (China). Phosphate-buffered saline (PBS; 0.1 mol·L^{-1}) was purchased from Sangon Bioengineering Co., Ltd. (China), and 5% Nafion solution was purchased from DuPont Co., Ltd.

LIG was prepared by means of a computer-controlled laser scribing micromachining system with a 10.6 μm CO_2 laser (50 W, PLS 6MW; Universal Laser Systems, USA). The morphology characterizations were obtained via scanning electron microscopy (SEM; SU8010; Hitachi, Japan), and the graphene structure was characterized by a Raman spectrometer (LabRAM HR; HORIBA Jobin Yvon, Japan). X-ray diffraction (XRD) was carried out using a D8 advance diffractometer (Bruker, Germany). Electrochemical characterizations were performed by a potentiostat (Sens 3; PalmSens, Netherlands). Ultraviolet (UV) spectroscopy was carried out by means of a microplate reader (BioTek, France). Deionized water was obtained using a Milli-Q purification system (Millipore, USA).

2.2. Preparation of LIG microelectrodes

The PI film was ultrasonically cleaned with ethanol and deionized water for 10 min each. The cleaned PI film was fixed onto the surface of a copper plate, and laser induced graphene sheet (LIGS) was induced on the PI film by the laser engraving machine. The implanted part of the microelectrode was 3 mm wide and 3 mm long. The diameter of the circular work area was 0.75 mm, and the widths of both the reference electrode and the counter electrode were 0.2 mm. The optimal laser power, velocity, and image density were 8%, 14%, and 750 pulses per inch (PPI), respectively. A mask layer (50 μm thick) made by laser cutting PI tape was laid on the surface of the PI substrate to protect the microelectrode from damage to the sensing layer when the microelectrode was pierced into a tomato stem. All laser engraving experiments were

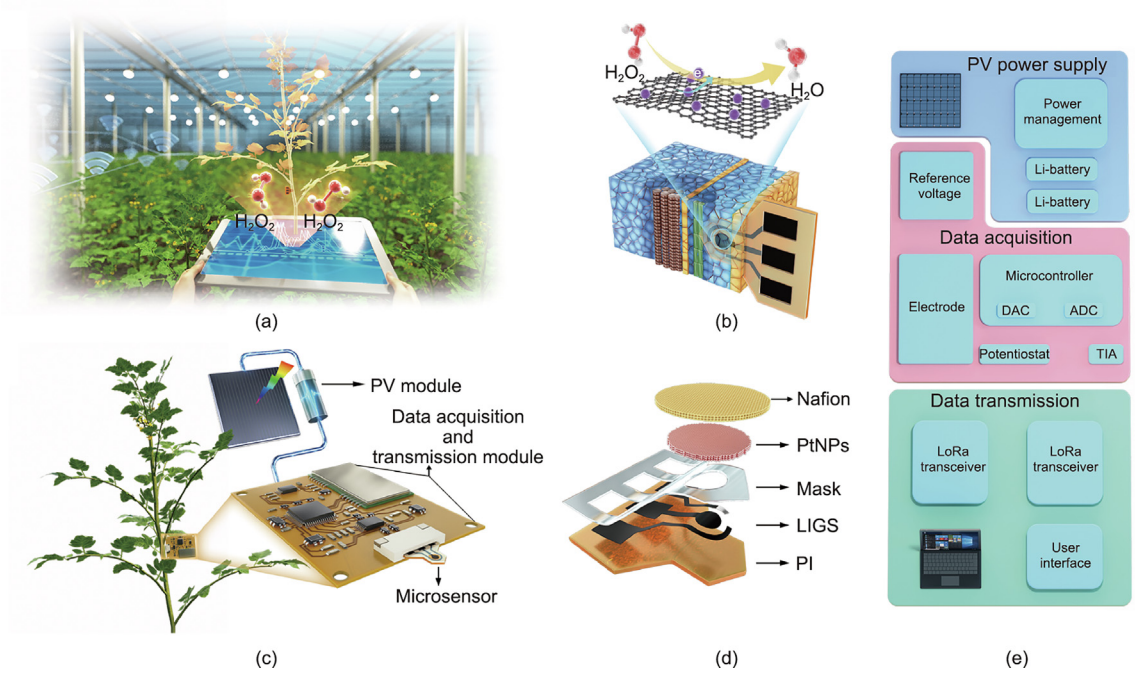

Fig. 1. Illustration of the implantable and self-powered sensing system. (a) Schematic illustration of the sensing system for the *in vivo* continuous monitoring of dynamic H_2O_2 in tomato plants; (b) cross-sectional illustration of the microsensor, with the microelectrode piercing the stem to reach the xylem; (c) main components of the sensing system; (d) exploded view of the microelectrode; (e) a system-level block diagram. PtNPs: platinum nanoparticles; LIGS: laser induced graphene sheet; PI: polyimide; DAC: digital-to-analog converter; ADC: analog-to-digital converter; TIA: transimpedance amplifier; LoRa: long range radio.

conducted in an air environment. A reference electrode was obtained by coating the reference area of the LIG with Ag/AgCl ink.

2.3. Preparation of microsensor and the electrochemical sensing method

An integrated three-electrode system based on LIGS was prepared according to the above steps. Before the modification of the sensing interface, the prepared electrode was electroactivated using the cyclic voltammetry (CV) method within five cycles in PBS electrolyte (with a voltage ranging from +0.3 to +1.4 V and a scan rate of 100 $mV \cdot s^{-1}$). Then, 5 μL of K_2PtCl_4 solution (2 $mmol \cdot L^{-1}$, dissolved in 0.1 $mol \cdot L^{-1}$ Na_2SO_4) was added to the three-electrode reaction region [29]. Platinum nanoparticles (PtNPs) were electrodeposited onto the interface of the LIGS via the CV method within seven cycles in a voltage range from −0.4 to +0.5 V to obtain the LIGS/PtNPs microelectrode (with a scan rate of 50 $mV \cdot s^{-1}$). Next, 0.4 μL of 0.2% Nafion solution was added onto the working electrode and the reference electrode to obtain the microsensor (LIGS/PtNPs/Nafion).

An electrochemical sensing method for H_2O_2 was established using a potentiostat; the electrochemical behavior of H_2O_2 was characterized by CV, and the detection potential of H_2O_2 was optimized by means of chronoamperometry (CA).

2.4. In vitro simulation

The purpose of the *in vitro* simulation was to simulate the intravital conditions of the tomato plant as much as possible and to investigate the feasibility of the microsensor for *in vivo* sensing. A tomato stem was cut off at 5 cm from the root, and the wound was covered with absorbent cotton and sealed with a plastic bag to prevent the fresh bleeding sap from evaporation [30]. The bleeding sap adsorbed by the cotton was squeezed out, collected in a centrifuge tube, and frozen at −20 °C for later use. Before use, the bleeding sap was filtered with a 0.22μm membrane filter to remove impurities [31] and then heated at 90 °C for half an hour to inactivate enzymes. H_2O_2 solutions were prepared with the treated bleeding sap as the solvent and were analyzed using the prepared microsensor.

2.5. In vivo *monitoring*

The tomato plants used for the osmotic stress testing were obtained through soilless cultivation, while the other tomato plants were cultivated in nutrient soil. All plants were cultivated in an environmentally controlled plant factory with a temperature of 26 °C, relative humidity (RH) of about 70%, and light intensity of 15 klx. Tomato plants with a height of about 30 cm were selected for monitoring. A 2 mm incision was carefully made with a scalpel on the tomato stem, and the microsensor was inserted into the incision to complete the implantation. Osmotic stress was induced by adding 30% PEG to the hydroponic nutrient solution. The tomato stem was clipped with hemostatic forceps to produce mechanical injury stress. Ultraviolet (UV) stress for the tomato plants was induced using UV lamps (λ = 368 nm).

2.6. Detection of H_2O_2 in tomato plants via UV spectroscopy

A tomato stem frozen in liquid nitrogen was ground immediately. Then 0.2 mL of TCA (0.1%) solution and 0.8 mL of KI (1 $mol \cdot L^{-1}$) solution were added to 200 mg of the crushed stem and mixed well with a vortex mixer. The mixture was centrifuged at 12 000*g* for 15 min. Then, 200 μL of supernatant was put in a 96-well plate to record the absorbance at 350 nm [32,33].

3. Results and discussion

3.1. Sensing system design

The core of the system is the LIG-based microsensor, which is composed of three layers: a PI substrate, a conductive and sensing layer, and a PI mask layer (Fig. 1(d); Fig. S1(a) in Appendix A). The conductive and sensing layer is made of 3D porous LIG, which is prepared on the surface of PI film using CO_2 LIG technology [13,34]. The 3D porous LIG provides a conductive substrate with a large surface area for the modification of PtNPs with electrocatalytic properties. A circular working area with a diameter of 500 μm is covered by electrodeposited PtNPs as an electrochemical sensing layer and a Nafion membrane as an anti-interference layer. To prevent mechanical damage to the sensing layer when the microsensor is inserted into the stem, a mask layer (50 μm thick) made by laser cutting PI tape is used to cover the surface of the PI substrate (Fig. S1(b) in Appendix A).

Traditional wearable plant sensors are powered by wired power sources or batteries. However, the presence of a large number of power lines and frequent battery replacements are not conducive to the continuous and stable operation of wearable plant sensors. Thus, providing a sustainable power supply without power lines or the need for battery replacement is both a crucial and challenging issue in the design of wearable plant sensors [1]. Sufficient light conditions in the crop-growing environment provide the possibility of a PV power supply. Therefore, a PV power supply module was designed, fabricated, and then combined with a data-acquisition and -transmission module to form a self-powered sensing system (Fig. 1(e)). The PV module, which has an output voltage of 6.0 V, can charge a 3.0 V lithium-ion (Li) battery by harvesting the available light energy in the agricultural environment. As shown in Fig. S2(a) in Appendix A, the red indicator light on the circuit board shows that the PV module can power the battery even under artificial light conditions (15 klx). In the data-acquisition module, the bias potential required for electrochemical measurements is derived from the voltage generated by the digital-to-analog converter (DAC) in the chip and the external reference voltage. The current of the microsensor is amplified and converted into a voltage signal through a transimpedance amplifier (TIA), and the voltage signal is converted into a digital voltage value after being read by the analog-to-digital converter (ADC) inside the microcontroller. In the data-transmission module, electrochemical data can be transmitted to the user interface by a long range radio (LoRa) network within 1000 m. Finally, the received voltage value is converted into the current value via software. Figs. S2(b) and (c) in the Appendix A illustrates the design of the whole electronic circuit and provides a picture of the entire system used for H_2O_2 monitoring in tomato plants.

3.2. Characterizations

As an electrochemical sensing platform, the 3D porous LIG provides a conductive substrate with a large surface area for the modification of noble-metal nanoparticles with electrocatalytic activity toward H_2O_2 and plays a crucial role in the sensitive detection of H_2O_2 [35–37]. By adjusting the laser power and scanning rate, LIG morphologies with fibers (LIGF), LIGS, and sheets mixed with fibers (LIGSF) can be obtained (Fig. 2(a); Fig. S3 in Appendix A) [38–40].

We found that more uniform PtNPs could be electrodeposited on the surface of LIGS (Fig. 2(b); Fig. S3). To explain this difference, LIGF, LIGS, and LIGSF were characterized using Raman spectroscopy and XRD. As shown in Fig. 2(d), the main differences according to Raman spectroscopy are the 2D band at 2658 cm^{-1},

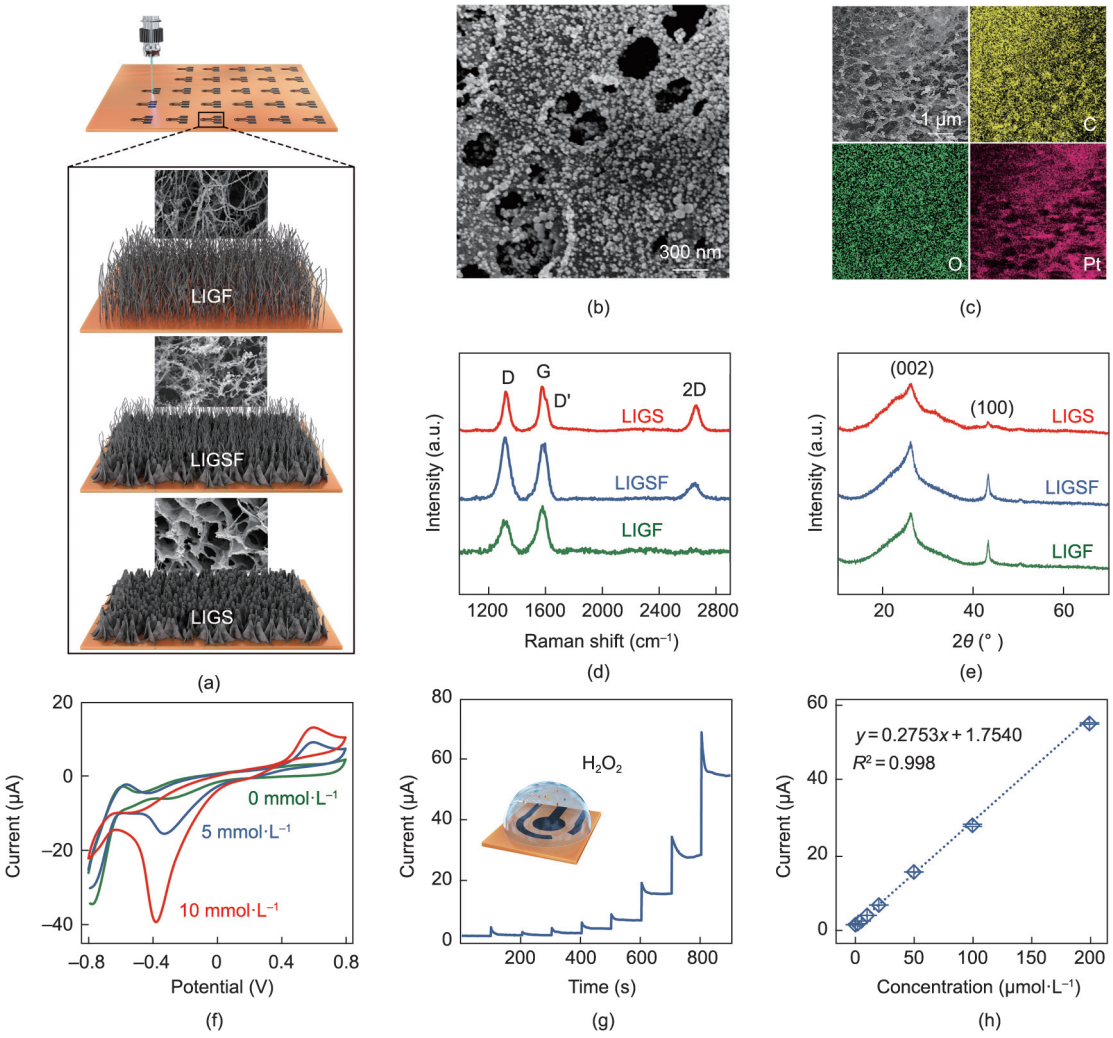

Fig. 2. Characterization and electrochemical performance of the microsensor. (a) Schematic illustration of the LIG morphologies of LIGF, LIGS, and LIGSF; (b) SEM images of LIGS/PtNPs; (c) corresponding elemental mapping of carbon (C), oxygen (O), and platinum (Pt); (d) Raman spectra of LIGF, LIGS, and LIGSF; (e) XRD analysis of LIGF, LIGS, and LIGSF; (f) CV curves for different concentrations of H_2O_2 on the LIGS/PtNPs/Nafion microsensor; (g) CA responses of H_2O_2 in the range of 2–200 μmol·L^{-1} on the LIGS/PtNPs/Nafion microsensor; (h) the corresponding calibration curve. *x*: the concentration of H_2O; *y*: the responses of microsensors; *R*: the related coefficient; a.u.: absorbance unit.

which corresponds to 3D multilayer graphene structures, and the D′ band at 1616 cm^{-1}, which corresponds to the edge defects of graphene. The LIGS have a higher 2D band and a more obvious D′ band than the LIGSF and LIGF, which indicates that the presence of fiber reduces the lamellar structure and edge defects of the graphene. As shown in Fig. 2(e), the LIGS have the lowest (100) peak at 43.1°, which reveals that the LIGS have a high-quality graphene crystal structure. Since electrochemical electron transfer commonly occurs at the edge defects, the presence of fibers in LIGF may induce a slower heterogeneous electron transfer rate, which is not conducive to the electrodeposition of PtNPs. The electrochemical performance of the LIG microelectrodes electrodeposited with PtNPs also confirmed that there were more PtNPs on the LIGS (Fig. S4 in Appendix A). Therefore, LIGS were chosen as the modification platform of PtNPs. Interestingly, we found that the electrochemical performance of LIGS could be improved by means of a simple electrochemical activation treatment (Fig. S5 in Appendix A), and the best electrochemical performance was achieved when the LIGS were electroactivated in PBS using CV within five cycles in a voltage range from +0.3 to +1.4 V. This phenomenon can be attributed to the fact that electrochemical activation can remove organic impurities at the LIGS surface to improve the electron transfer rate. In addition, we investigated the electrodeposition conditions of the PtNPs, including the electrolyte and the number of electrodeposition cycles, by means of SEM and electrochemical characterizations. Based on the SEM (Fig. S6 in Appendix A) and electrochemical (Fig. S7 in Appendix A) results, the optimal electrodeposition conditions for the PtNPs on LIGS are the CV method within seven cycles in Na_2SO_4 electrolyte.

After preparing the PtNPs on the surface of the LIGS (denoted as LIGS/PtNPs), an anti-interference layer of Nafion film was coated onto the surface of the LIGS/PtNPs (denoted as LIGS/PtNPs/Nafion) to obtain a microsensor that could be implanted. The Nafion film, which has a negative charge, repels anionic interferents, and its self-adhesion enhances the stability of the interface [41,42]. Prior to investigating the detection performance of the LIGS/PtNPs/Nafion microsensor, we examined the electrocatalytic behavior of the microsensor toward H_2O_2. As shown in Fig. 2(f), the CV curves for different concentrations of H_2O_2 indicate that H_2O_2 undergoes electrochemical oxidation at +0.6 V and electrochemical reduction at −0.4 V. To avoid interference from dissolved oxygen, the oxidation potential was selected as the applied potential for the CA method [36]. The CA responses of H_2O_2 under different potentials were investigated, and the highest response value was obtained at +0.6 V (Fig. S8 in Appendix A). Therefore, +0.6 V was selected as the optimal potential for the CA method. As shown in

Figs. 2(g) and (h), under the optimal detection conditions, the LIGS/PtNPs/Nafion microsensor exhibited a good linear relationship with H_2O_2 in the range of 2–200 μmol·L^{-1}. The limit of detection (LoD) was calculated to be 0.35 μmol·L^{-1}, according to the equation LoD = 3Sb/*m*, where Sb and *m* represent the standard deviation of the blank signals and the slope of the calibration curve, respectively.

3.3. Anti-interference performance and repeatability

The anti-interference performance of the microsensor against chemical interferents was investigated. The H_2O_2 produced in plants can cause an increase in the content of ascorbic acid (AsA), which has antioxidant properties. AsA has a wide potential window and is the main chemical interferent in the electrochemical detection of H_2O_2 (Fig. S9(a) in Appendix A) [43]. As shown in Fig. S9(b) in Appendix A, the LIGS/PtNPs/Nafion microsensor exhibited no response to AsA (50 μmol·L^{-1}), while maintaining the highest response to H_2O_2 (Fig. S9(c) in Appendix A). In addition, K^+, Na^+, Ca^{2+}, glucose (Glu), and sucrose (Suc) were selected as interferents, and the response of the microsensor to the individual interferents and to a mixture of these interferents was investigated. As shown in Figs. 3(a) and (b), the interference had little effect on the response of the microsensor. Five microsensors were selected to detect the same concentration of H_2O_2, and the relative standard deviation (RSD) of the response was 3.5% (Fig. 3(c)), indicating satisfactory repeatability.

It has been reported that the pH of tomato plants is commonly in the range of 5.0–8.0 [44]. Therefore, it was necessary to investigate the effect of pH fluctuation on the response of the microsensor. In the range of pH 5.0–8.0, with an interval of 0.5, the CA responses of the LIGS/PtNPs/Nafion microsensor to H_2O_2 with a concentration of 100 μmol·L^{-1} were investigated. As shown in Fig. 3(d), the response fluctuate of the LIGS/PtNPs/Nafion microsensor fell within a certain range (RSD = 6.2%). The pH tolerance of the microsensor can be attributed to the Nafion layer on the Ag/AgCl reference electrode, as a bare Ag/AgCl reference electrode can be affected by the pH, resulting in a shift in the oxidation potential. The use of a Nafion film has been demonstrated to reduce the potential shift to 13 mV over a pH range of 4.0–10.0 [45].

Normal plant growth is inseparable from temperature difference. Therefore, it was necessary to investigate the effect of temperature difference on the response of the LIGS/PtNPs/Nafion microsensor. The CA responses of the microsensor at 17, 20, 25, 30, and 35, and 35°C were investigated in PBS electrolyte. As

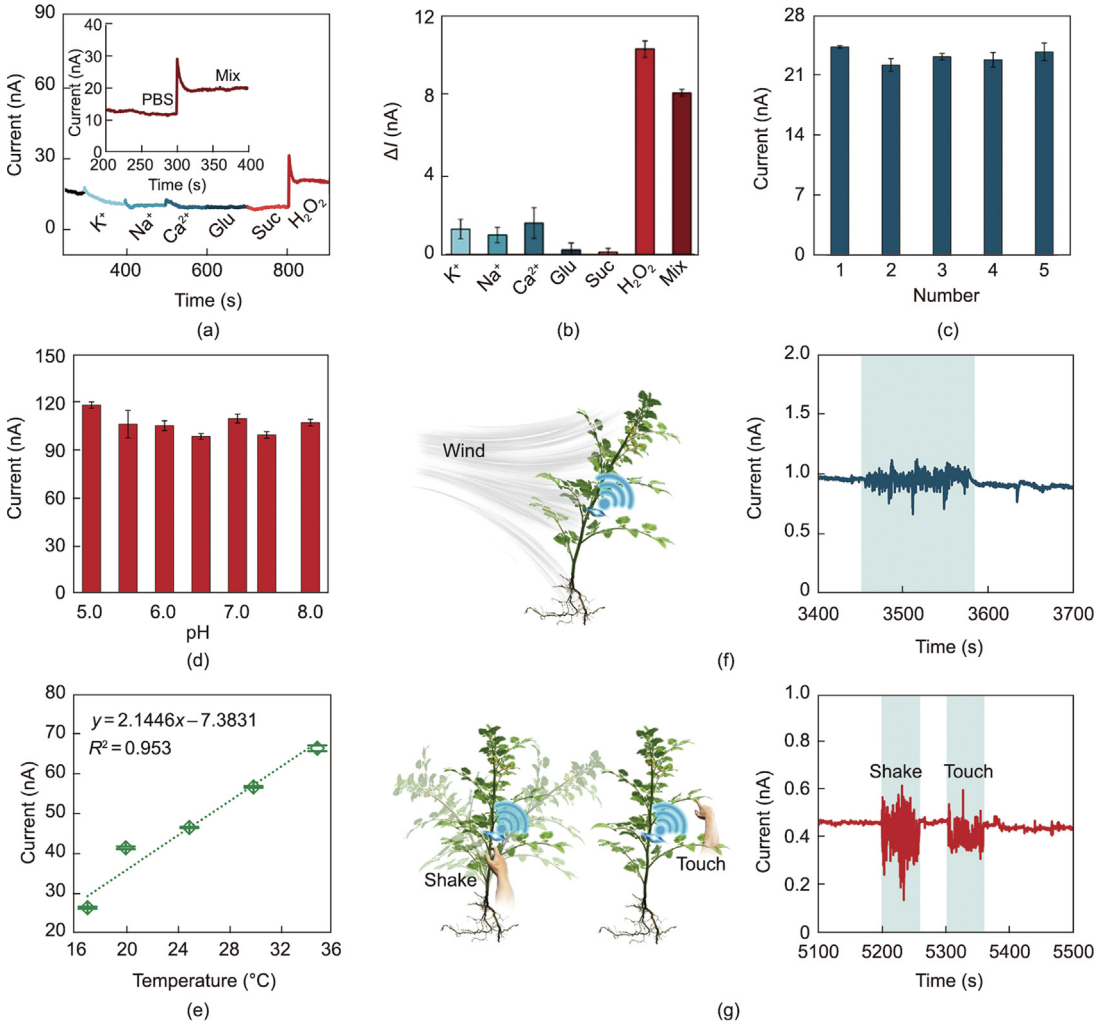

Fig. 3. Anti-interference performance and repeatability. (a, b) The anti-interference performance of the microsensor against chemical interferents (100 μmol·L^{-1} K^+, Na^+, Ca^{2+}, Glu, and Suc; 10 μmol·L^{-1} H_2O_2, the Δ*I* is the variation of currents); (c) responses of five microsensors to 10 μmol·L^{-1} H_2O_2; (d) response of the microsensor to 100 μmol·L^{-1} H_2O_2 with different pH values; (e) response of the microsensor in PBS at 17, 20, 25, 30, and 35°C; (f) effects of air flow (1.5 m·s^{-1}) on the performance of the microsensor implanted into a tomato stem; (g) effects of mechanical disturbance on the performance of the microsensor implanted into a tomato stem.

shown in Fig. 3(e), the response increased with an increase in temperature, due to the increased conductivity caused by the increased electron–phonon scattering and thermal velocity of the electrons [34,46]. A relationship curve between the microsensor response and the ambient temperature was established for temperature calibration.

Air flow and mechanical disturbance commonly exist in the planting environment. Therefore, the response of the LIGS/PtNPs/Nafion microsensor implanted into the tomato stem to an air flow of 1.5 m•s^{-1}, shaking the stem, and touching the leaves was investigated [12]. As shown in Figs. 3(f) and (g), the microsensor exhibited a certain degree of fluctuation. After the disturbance was eliminated, the response of the microsensor immediately recovered and became stable. The fluctuation might be caused by a relative displacement between the sensor and the plant tissue, which can be avoided by means of a stable fixation method or an interface with strong tissue adhesion.

3.4. In vitro *simulation*

As the microsensor is a mini-invasive sensing tool, its sensing interface comes into direct contact with the plant's phloem and xylem sap. The complex contents of the sap may block the normal operation of the microsensor. Thus, it was necessary to study the blocking effect of plant sap on the H_2O_2 signal, in order to obtain a calibration method for the accurate quantitative analysis of H_2O_2 *in vivo*. The bleeding sap of tomato plants was collected according to the steps shown in Fig 4(a), and different concentrations of H_2O_2 were added to the bleeding sap to be analyzed by the LIGS/PtNPs/Nafion microsensor. When H_2O_2 was directly added to the bleeding sap without any pretreatment, the lowest concentration that could be measured was about 100 μmol•L^{-1} (Figs. 4(b) and (c)). This is likely because the peroxidase in the bleeding sap catalyzes the decomposition of the added H_2O_2. This result indirectly demonstrated that the LIGS/PtNPs/Nafion microsensor is specific to H_2O_2 and has the potential to detect peroxidase activity. Next, the fresh bleeding fluid was heated to inactivate the peroxidase, and H_2O_2 was added to the treated bleeding sap. The response of the microsensor to the bleeding sap is shown in Fig. 4(d); the minimum concentration of H_2O_2 detected was 5 μmol•L^{-1}. Fig. 4(e) shows the calibration curve based on the absolute response of the microsensor and H_2O_2 concentration. The results show that the microsensor is sensitive to 5–200 μmol•L^{-1} H_2O_2, with a good linear relationship. However, due to biodiversity, the baseline responses may differ in actual monitoring. It is difficult to perform a quantitative analysis using the absolute response. Thus, in order to solve quantitative problems, a calibration curve was drawn using the change rate of the current ($\Delta I/I_0$) and the H_2O_2 concentration (Fig. 4(f)). This made it possible to effectively deduct the difference in background signals between plants and improve the quantitative accuracy of the actual monitoring results.

3.5. In vivo *monitoring*

The various environmental factors causing harm to plants, such as drought, salinity, radiation, pests, weeds, or rodents, are collectively referred to as stress [16,47]. Stress can be divided into abiotic stress and biological stress. Abiotic stress, which includes drought, salt, UV radiation, and mechanical injury caused by insect feeding, can limit crop production and threaten national food security [19]. Thus, the self-powered sensing system was used to monitor the dynamic H_2O_2 levels in tomato plants in real time under osmotic, UV, and mechanical injury stress.

Drought and salt mainly lead to hyperosmotic stress, which is usually referred to as osmotic stress [18]. Osmotic stress can increase the abscisic acid (ABA) content in plants. SnRK2s (protein kinase) activated by ABA can phosphorylate RbOHF (NADPH oxidase) to generate $O_2^{\cdot-}$ in the exosome space and then form H_2O_2.

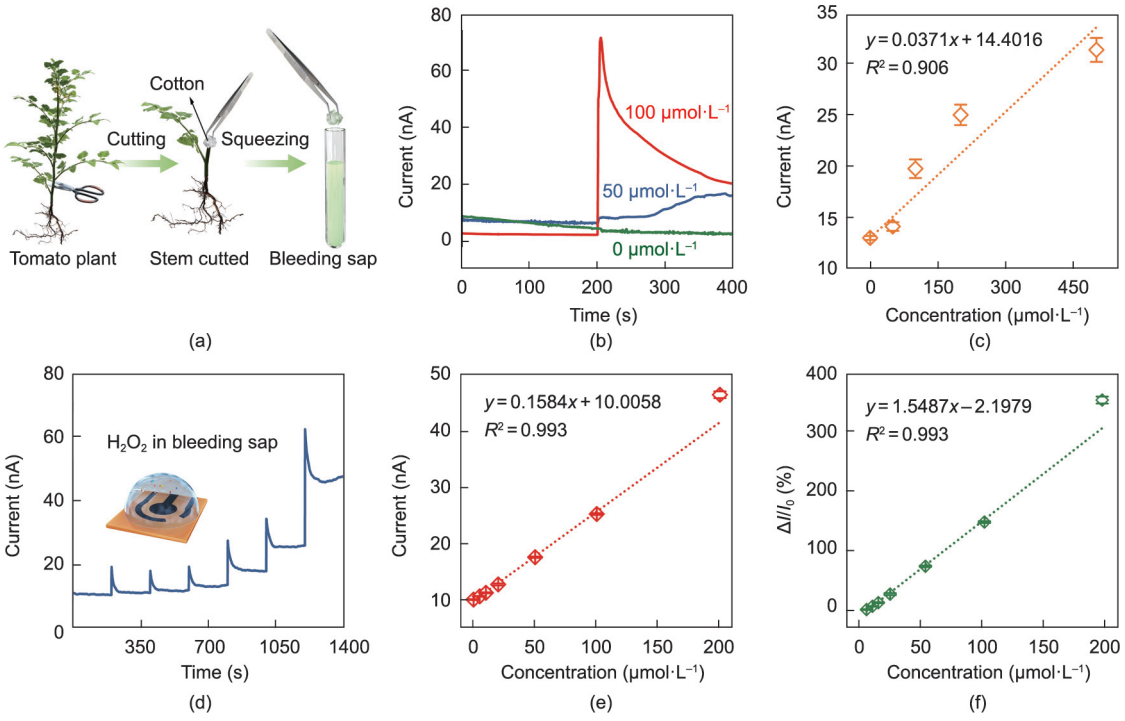

Fig. 4. The *in vitro* simulation tests. (a) Schematic illustration of the *in vitro* simulation tests; (b) response of the microsensor to H_2O_2 in the bleeding sap without any pretreatment; (c) calibration curve of H_2O_2 in the bleeding sap without any pretreatment (50–500 μmol•L^{-1}); (d) CA responses of H_2O_2 in the pretreated bleeding sap (2–200 μmol•L^{-1}); (e) corresponding calibration curve based on the absolute response value of the microsensor and H_2O_2 concentration; (f) corresponding calibration curve based on $\Delta I/I_0$ and the H_2O_2 concentration.

As shown in Fig. 5(a), the microsensor was implanted into a tomato stem to monitor the H_2O_2 signal. Tomato plants were cultured in hydroponic nutrient solution containing 30% PEG to induce osmotic stress [48,49]. The monitoring results are shown in Fig. 5(b). An H_2O_2 signal peak was obtained at 12.5 h (after 7.5 h of osmotic stress), which was denoted as the oxygen burst. The H_2O_2 signal then continued for about 6.5 h. In the control group, the monitoring signals of the tomato plants without osmotic stress remained stable. As shown in Fig. 5(c), another tomato plant was subjected to osmotic stress after 5 h of cultivation; the H_2O_2 signal increased and reached a peak at 18 h, at which time the top of the tomato plant was obviously withered. At 19 h, the PEG solution was extracted, and fresh hydroponic nutrient solution was injected to relieve the osmotic stress. It was observed that the H_2O_2 signal then began to decline, with another intense oxygen burst occurring at 23 h. This oxygen burst lasted for about 19 h. At 42 h, the signal began to stabilize. At this time, the tomato plant had recovered its fresh state. Furthermore, the microsensor monitoring the tomato plants without osmotic stress exhibited a stable response for 50 h (the fluctuations around 24 and 40 h might be caused by vibration during manual farming operations). After monitoring for 50 h, the microsensor was removed and used to detect 100 μmol·L^{-1} H_2O_2 added to bleeding sap. The H_2O_2 concentration was quantitatively calculated based on the calibration curve in Fig. 4(f) and was found to be 88.33 μmol·L^{-1}, indicating that the microsensor still maintained adequate analytical performance after working for 50 h (Fig. S10 in Appendix A).

Mechanical injury can induce a rapid H_2O_2 signal [50,51]. Therefore, it is convenient to use mechanical injury stress monitoring to study the spatial and temporal distribution of H_2O_2 signals in plants. As shown in Fig. 5(d), the microsensor was implanted into a tomato stem at about 10 cm above the root. The side branches, leaves, and main stem were clamped by hemostatic forceps to form mechanical injuries. As shown in Fig. 5(e) and Figs. S11(a)–(c) in Appendix A, the injured main stem and side branches generated several H_2O_2 signals within minutes, which is difficult to capture using conventional detection methods. The microsensor was unable to obtain the H_2O_2 signals caused by the mechanical injury applied to the leaves, similar to a previous study [19]. The H_2O_2 produced in the leaves might have been decomposed during the

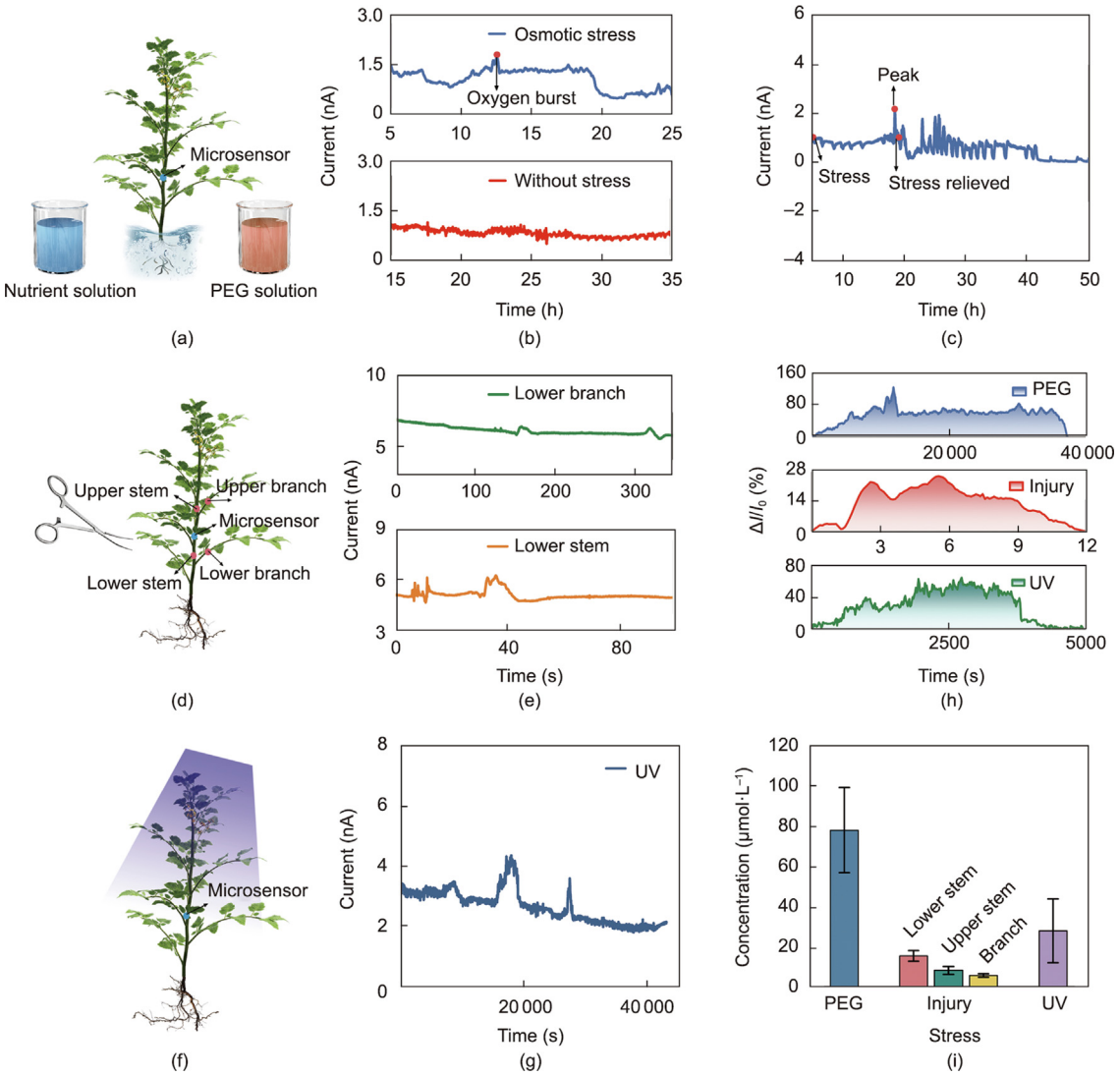

Fig. 5. *In vivo* performance of the implantable and self-powered sensing system. (a) Schematic illustration of the sensing system for the monitoring of osmotic stress; (b) corresponding monitoring curves of H_2O_2 in tomato plants with and without osmotic stress; (c) corresponding monitoring curves of H_2O_2 in tomato plants with osmotic stress and with that stress relieved; (d) schematic illustration of the sensing system for the monitoring of mechanical injury; (e) corresponding monitoring curves of H_2O_2 in different tissue parts of tomato plants with mechanical injury; (f) schematic illustration of the sensing system for the monitoring of UV stress; (g) corresponding monitoring curves of H_2O_2 under UV stress; (h) wave characteristics of the H_2O_2 signal under various stresses; (i) changes in the H_2O_2 content in tomato plants under various stresses.

transmission process, leaving insufficient to be transmitted to the microsensor implantation site.

The distance between the position of the injury and the microsensor and the time required for the H_2O_2 signal to appear were recorded in order to calculate the transmission rate of H_2O_2. As shown in Fig. S11(d) in Appendix A, the transmission rate of the H_2O_2 signal generated above the microsensor was the fastest (1.58 mm•s^{-1}), while the transmission rate of the H_2O_2 signal generated by the side branches was the lowest (0.23 mm•s^{-1}). To demonstrate that the generated signal originated from H_2O_2, active oxygen inhibitors were injected into the stem during the monitoring, including peroxidase (CAT), diphenyleneiodonium (DPI), and $LaCl_3$. As shown in Fig. S12 in Appendix A, no H_2O_2 signal was observed during the monitoring.

Light is important for crop growth. In recent years, due to the destruction of the ozone layer, the UV light reaching the earth's surface has gradually increased [52,53]. Too much UV light causes stress effects on crop growth [52,54]. As shown in Fig. 5(f), UV light radiation (365 nm) was applied to form stress on tomatoes. As shown in Fig. 5(g), an H_2O_2 signal lasting for a few minutes appeared three times. It is worth noting that the response curve had some noise, which might be caused by interference from UV light with electromagnetic wave properties.

It can be seen from the above results that an H_2O_2 signal is an early response of plants to stress that can be generated within a few minutes. The wave characteristics of the H_2O_2 signal under various stresses were compared. As shown in Fig. 5(h), the H_2O_2 signal caused by osmotic stress can last for tens of hours, while the H_2O_2 signal caused by mechanical injury stress only lasts for tens of seconds, and that caused by UV stress lasts for tens of minutes. Finally, according to the quantitative calibration curve in Fig. 4(f), we calculated the concentration of the H_2O_2 signal generated by the above stresses. The results are shown in Fig. 5(i). The H_2O_2 concentration generated by various stresses basically ranged within 10–100 μmol•L^{-1}, which is consistent with the conclusions reported in the literature [19,20]. It is clear that the H_2O_2 waves generated by plants in response to various stresses are different in terms of both time dimension and concentration. To further verify the accuracy of this method, the H_2O_2 content in tomato plants before and after osmotic stress was analyzed by means of UV spectrophotometry (Fig. S13 in Appendix A). The results showed that the H_2O_2 content after osmotic stress increased by 89 μmol•L^{-1}, in comparison with the result obtained from the sensing system of 78 μmol•L^{-1}. The difference in these values might be caused by biodiversity and the sample treatment.

In conclusion, we found that the tomato plants have the fastest response but weakest response intensity to mechanical damage. The response speed to osmotic stress was the slowest, but the response intensity was the largest. These results may demonstrate the time and concentration specificity of the H_2O_2 signal in response to abiotic stress, indicating that tomato plants can easily cope with some mechanical injury in daily growth. However, under osmotic stress and UV light, once the stress intensity exceeds the tolerance limit of the tomato plants, the plants produce a high-intensity H_2O_2 signal to resist stress damage.

4. Conclusions

It is necessary to analyze the breeding target traits and crucial biochemical molecules in plants via micro, dynamic, continuous, accurate, and intravital methods. H_2O_2 is a key early signal molecule for plants dealing with various stressors and has the characteristics of fast, long-distance, and automatic transmission. In this work, we developed an implantable and self-powered sensing system for the *in vivo* monitoring of the dynamic H_2O_2 level in a plant. Using this system, the transmission process of the H_2O_2 signal was monitored and analyzed *in vivo*, and the time and concentration specificity of the H_2O_2 signal for abiotic stress were investigated. The system has the following advantages:

(1) It can convert the H_2O_2 signal into a readable electrochemical signal both *in vivo* and in real time;

(2) The sensing system has a high time resolution (0.1 s);

(3) There is no need to inject various marking materials into the plant being monitored;

(4) The sensing system possesses anti-interference capability against environmental changes;

(5) Power from sunlight or artificial light in the agricultural environment can be fully utilized to continuously power the sensing system.

The results showed that this system can continuously monitor the H_2O_2 level in tomato plants under abiotic stress, including osmotic stress, mechanical damage, and UV radiation. The transmission process of the H_2O_2 signal was monitored and analyzed *in vivo*, and the content and waveform differences in H_2O_2 caused by different abiotic stresses were compared. We also investigated the time and concentration specificity of the H_2O_2 signal for abiotic stress. The system provides an advanced analysis tool for plant stress-resistance breeding and the early sensing diagnosis of plant stress in facility agriculture. In future, a more stable fixation method, stronger tissue adhesion, a reduction of baseline drift and noise, and the effect of device implantation on plant growth will be researched.

Declaration of competing interest

The authors declare that they have no known competing financial interests or personal relationships that could have appeared to influence the work reported in this paper.

Acknowledgments

This research was supported by the Joint Funds of the National Natural Science Foundation of China (U23A20173) and the Fundamental Research Funds for the Central Universities.

Appendix A. Supplementary data

Supplementary data to this article can be found online at https://doi.org/10.1016/j.eng.2023.11.021.

References

[1] Lee G, Wei QS, Zhu Y. Emerging wearable sensors for plant health monitoring. Adv Funct Mater 2021;31(52):2106475.
[2] Oren S, Ceylon H, Schnable PS, Dong L. High-resolution patterning and transferring of graphene-based nanomaterials onto tape toward roll-to-roll production of tape-based wearable sensors. Adv Mater Technol 2017;2(12):1700223.
[3] Koman VB, Lew TTS, Wong MH, Kwak SY, Giraldo JP, Strano MS. Persistent drought monitoring using a microfluidic-printed electro-mechanical sensor of stomata in planta. Lab Chip 2017;17(23):4015–24.
[4] Lan L, Le X, Dong H, Xie J, Ying Y, Ping J. One-step and large-scale fabrication of flexible and wearable humidity sensor based on laser-induced graphene for real-time tracking of plant transpiration at bio-interface. Biosens Bioelectron 2020;165:112360.
[5] Lu Y, Xu K, Zhang L, Deguchi M, Shishido H, Arie T, et al. Multimodal plant healthcare flexible sensor system. ACS Nano 2020;14(9):10966–75.
[6] Chai Y, Chen C, Luo X, Zhan S, Kim J, Luo J, et al. Cohabiting plant-wearable sensor *in situ* monitors water transport in plant. Adv Sci 2021;8(10):2003642.
[7] Luo Y, Li W, Lin Q, Zhang F, He K, Yang D, et al. A morphable ionic electrode based on thermogel for non-invasive hairy plant electrophysiology. Adv Mater 2021;33(14):e2007848.

[8] Tang WZ, Yan TT, Wang F, Yang JX, Wu J, Wang JL, et al. Rapid fabrication of wearable carbon nanotube/graphite strain sensor for real-time monitoring of plant growth. Carbon 2019;147:295–302.
[9] Nassar JM, Khan SM, Villalva DR, Nour MM, Almuslem AS, Hussain MM. Compliant plant wearables for localized microclimate and plant growth monitoring. npj Flex Electron 2018;2(1):24.
[10] Zhang C, Zhang C, Wu XY, Ping JF, Ying YB. An integrated and robust plant pulse monitoring system based on biomimetic wearable sensor. npj Flex Electron 2022;6(1):43.
[11] Li Z, Paul R, Ba Tis T, Saville AC, Hansel JC, Yu T, et al. Non-invasive plant disease diagnostics enabled by smartphone-based fingerprinting of leaf volatiles. Nat Plants 2019;5(8):856–66.
[12] Li Z, Liu YX, Hossain O, Paul R, Yao SS, Wu S, et al. Real-time monitoring of plant stresses via chemiresistive profiling of leaf volatiles by a wearable sensor. Matter 2021;4(7):2553–70.
[13] Zhao F, He J, Li X, Bai Y, Ying Y, Ping J. Smart plant-wearable biosensor for *in-situ* pesticide analysis. Biosens Bioelectron 2020;170:112636.
[14] Devireddy AR, Zandalinas SI, Fichman Y, Mittler R. Integration of reactive oxygen species and hormone signaling during abiotic stress. Plant J 2021;105 (2):459–76.
[15] Giraldo JP, Wu H, Newkirk GM, Kruss S. Nanobiotechnology approaches for engineering smart plant sensors. Nat Nanotechnol 2019;14(6):541–53.
[16] Fichman Y, Mittler R. Rapid systemic signaling during abiotic and biotic stresses: is the ROS wave master of all trades? Plant J 2020;102 (5):887–96.
[17] Wang G, Hu C, Zhou J, Liu Y, Cai J, Pan C, et al. Systemic root–shoot signaling drives jasmonate–based root defense against nematodes. Curr Biol 2019;29 (20):3430–8.
[18] Zhu JK. Abiotic stress signaling and responses in plants. Cell 2016;167 (2):313–24.
[19] Wu H, Nißler R, Morris V, Herrmann N, Hu P, Jeon SJ, et al. Monitoring plant health with near-infrared fluorescent H_2O_2 nanosensors. Nano Lett 2020;20 (4):2432–42.
[20] Lew TTS, Koman VB, Silmore KS, Seo JS, Gordiichuk P, Kwak SY, et al. Real-time detection of wound-induced H_2O_2 signalling waves in plants with optical nanosensors. Nat Plants 2020;6(4):404–15.
[21] Zhang Q, Ying YB, Ping JF. Recent advances in plant nanoscience. Adv Sci 2022;9(2):2103414.
[22] Xia XJ, Wang YJ, Zhou YH, Tao Y, Mao WH, Shi K, et al. Reactive oxygen species are involved in brassinosteroid-induced stress tolerance in cucumber. Plant Physiol 2009;150(2):801–14.
[23] Wang CJ, Zhou ZG, Holmqvist A, Zhang H, Li Y, Adell G, et al. Survivin expression quantified by Image Pro-Plus compared with visual assessment. Appl Immunohistochem Mol Morphol 2009;17(6):530–5.
[24] Brennan T, Frenkel C. Involvement of hydrogen peroxide in the regulation of senescence in pear. Plant Physiol 1977;59(3):411–6.
[25] Zhou J, Zhou S, Fan P, Li X, Ying Y, Ping J, et al. Implantable electrochemical microsensors for *in vivo* monitoring of animal physiological information. Nano-Micro Lett 2024;16(1):49.
[26] Gao X, Ma W, Mao J, He CT, Ji W, Chen Z, et al. A single-atom Cu–N_2 catalyst eliminates oxygen interference for electrochemical sensing of hydrogen peroxide in a living animal brain. Chem Sci 2021;12(45):15045–53.
[27] Pan C, Wu F, Mao J, Wu W, Zhao G, Ji W, et al. Highly stable and selective sensing of hydrogen sulfide in living mouse brain with NiN_4 single-atom catalyst-based galvanic redox potentiometry. J Am Chem Soc 2022;144 (32):14678–86.
[28] Zhou S, Zhou J, Pan Y, Wu Q, Ping J. Wearable electrochemical sensors for plant small-molecule detection. Trends Plant Sci 2024;29(2):219–31.
[29] Xu J, Cheng C, Li X, Lu Y, Hu S, Liu G, et al. Implantable platinum nanotree microelectrode with a battery-free electrochemical patch for peritoneal carcinomatosis monitoring. Biosens Bioelectron 2021;185:113265.
[30] Nakano A, Higashide T, Ahn DH. Relationships between yield, mineral content of fruits, and sap bleeding rate in Dutch and Japanese tomato cultivars. Jarq-Jpn Agr Res Q 2017;51(1):69–75.
[31] Zheng T, Haider MS, Zhang KK, Jia HF, Fang JG. Biological and functional properties of xylem sap extracted from grapevine (cv. *Rosario bianco*). Sci Hortic 2020;272:109563.
[32] Ibrahim MH, Jaafar HZE. Primary, secondary metabolites, H_2O_2, malondialdehyde and photosynthetic responses of *Orthosiphon stimaneus* Benth. to different irradiance levels. Molecules 2012;17(2):1159–76.
[33] Junglee S, Urban L, Sallanon H, Lopez-Lauri F. Optimized assay for hydrogen peroxide determination in plant tissue using potassium iodide. Am J Anal Chem 2014;5(11):730–6.
[34] Yang Y, Song Y, Bo X, Min J, Pak OS, Zhu L, et al. A laser-engraved wearable sensor for sensitive detection of uric acid and tyrosine in sweat. Nat Biotechnol 2020;38(2):217–24.
[35] Zhang C, Ping J, Ying Y. Evaluation of *trans*-resveratrol level in grape wine using laser-induced porous graphene-based electrochemical sensor. Sci Total Environ 2020;714:136687.
[36] Lu Z, Wu L, Dai X, Wang Y, Sun M, Zhou C, et al. Novel flexible bifunctional amperometric biosensor based on laser engraved porous graphene array electrodes: highly sensitive electrochemical determination of hydrogen peroxide and glucose. J Hazard Mater 2021;402:123774.
[37] Yao Y, Lan LY, Liu XX, Ying YB, Ping JF. Spontaneous growth and regulation of noble metal nanoparticles on flexible biomimetic Mxene paper for bioelectronics. Biosens Bioelectron 2020;148:111799.
[38] Wan ZF, Umer M, Lobino M, Thiel D, Nguyen NT, Trinchi A, et al. Laser induced self-N-doped porous graphene as an electrochemical biosensor for femtomolar mirna detection. Carbon 2020;163:385–94.
[39] He MH, Wang YN, Wang SR, Luo SD. Laser-induced graphene enabled 1D fiber electronics. Carbon 2020;168:308–18.
[40] Duy LX, Peng ZW, Li YL, Zhang JB, Ji YS, Tour JM. Laser-induced graphene fibers. Carbon 2018;126:472–9.
[41] Mohan AMV, Windmiller JR, Mishra RK, Wang J. Continuous minimally-invasive alcohol monitoring using microneedle sensor arrays. Biosens Bioelectron 2017;91:574–9.
[42] Yu Y, Nassar J, Xu C, Min J, Yang Y, Dai A, et al. Biofuel-powered soft electronic skin with multiplexed and wireless sensing for human−machine interfaces. Sci Robot 2020;5(41):eaaz7946.
[43] Lowry JP, McAteer K, Elatrash SS, Duff A, Oneill RD. Characterization of glucose oxidase-modified poly(phenylenediamine)-coated electrodes *in–vitro* and *in–vivo*–homogeneous interference by ascorbic-acid in hydrogen-peroxide detection. Anal Chem 1994;66(10):1754–61.
[44] Wilkinson S, Corlett JE, Oger L, Davies WJ. Effects of xylem pH on transpiration from wild-type and *flacca* tomato leaves. A vital role for abscisic acid in preventing excessive water loss even from well-watered plants. Plant Physiol 1998;117(2):703–9.
[45] Nolan MA, Tan SH, Kounaves SP. Fabrication and characterization of a solid state reference electrode for electroanalysis of natural waters with ultramicroelectrodes. Anal Chem 1997;69(6):1244–7.
[46] Alahi MEE, Nag A, Mukhopadhyay SC, Burkitt L. A temperature-compensated graphene sensor for nitrate monitoring in real-time application. Sens Actuators A Phys 2018;269:79–90.
[47] Li H, Testerink C, Zhang Y. How roots and shoots communicate through stressful times. Trends Plant Sci 2021;26(9):940–52.
[48] Zhang C, Shi S. Physiological and proteomic responses of contrasting alfalfa (*Medicago sativa* L.) varieties to PEG-induced osmotic stress. Front Plant Sci 2018;9:242.
[49] Zhang H, Wang MJ, Hu LY, Wang SH, Hu KD, Bao LJ, et al. Hydrogen sulfide promotes wheat seed germination under osmotic stress. Russ J Plant Physiol 2010;57(4):532–9.
[50] Cordeiro JV, Jacinto A. The role of transcription-independent damage signals in the initiation of epithelial wound healing. Nat Rev Mol Cell Biol 2013;14 (4):249–62.
[51] Hu YP, Peng YB, Zhang YF, Wang Y, Yu WR, Yao M, et al. Reactive oxygen species mediated prostaglandin E_2 contributes to acute response of epithelial injury. Oxid Med Cell Longev 2017;2017:4123854.
[52] Takshak S, Agrawal SB. Defense potential of secondary metabolites in medicinal plants under UV-B stress. J Photochem Photobiol B 2019;193:51–88.
[53] Dmytriiev OP, Hushcha MI. Effect of UV-B radiation on cytophysiological responses in plants. Tsitol Genet 2003;37(6):66–77.
[54] Fu G, Shen ZX. Effects of enhanced UV-B radiation on plant physiology and growth on the Xizang Plateau: a meta-analysis. Acta Physiol Plant 2017;39 (3):85.